Ionic Conductivitiy and Structure of $(LiCl)_2$–Al_2O_3–SiO_2 Xerogels

B. Wang, S. Szu,† and M. Greenblatt*

Department of Chemistry, Rutgers—The State University of New Jersey, Piscataway, New Jersey 08855-0939

L. C. Klein

Department of Ceramics, Rutgers—The State University of New Jersey, Piscataway, New Jersey 08855-0909

Received September 9, 1991. Revised Manuscript Received November 15, 1991

$(LiCl)_2$–Al_2O_3–SiO_2 xerogels were prepared by a sol–gel process. The structure of the heat-treated xerogels was studied by powder X-ray diffraction, Fourier transform infrared spectroscopy, and ^7Li, ^{29}Si, and ^{27}Al nuclear magnetic resonance techniques. ^7Li NMR studies indicate two kinds of lithium ions in the xerogels: (a) polycrystalline LiCl dispersed in the pores of the xerogel and (b) lithium ions associated with nonbridging oxygens on the silica tetrahedra or associated with AlO_4^- units. For the samples having the same lithium content (20 mol % $(LiCl)_2$) the ionic conductivity increases with increasing Al_2O_3/SiO_2 ratio. This is attributed to the increasing concentration of lithium ions associated with tetrahedral AlO_4 or nonbridging oxygens in the xerogel. A constant activation energy is observed when the $(LiCl)_2$ content increases from 10 to 20 mol % for samples having the sample Al_2O_3/SiO_2 ratio of 1/2. This constant activation energy is analyzed in terms of the competition between the decreasing jump distance tending to decrease activation energy and increasing Coulombic interaction tending to increase activation energy.

Introduction

Lithium aluminosilicate glasses with high ionic conductivity recently have attracted a great deal of interest.[1-3] In particular, high Li^+ ion conductivity was reported in a lithium aluminosilicate glass with the β-eucryptite composition ($Li_2O{\cdot}Al_2O_3{\cdot}2SiO_2$ or $LiAlSiO_4$).[2,3] Pechenik et al.[3] studied the mechanism of ionic motion in $LiAlSiO_4$ glass using a combination of structural and transport methods. These glasses were prepared by a conventional melt–quench method. Alternatively, similar compositions can be prepared by the sol–gel process, which is a low temperature approach to glass formation. The sol–gel process can be used when the melting temperature is high as in the case of lithium aluminosilicate glasses (~1600 °C). For lithium aluminosilicate gels the role of alcohol, the crystallization behavior, shrinkage, and precursor residue have been studied previously.[4-7]

Since glasses prepared by a sol–gel technique are initially less dense than those prepared by conventional melt–quench techniques, samples prepared by a sol–gel technique may provide a greater free volume through which conducting ions can move. Recently, ionic conductivities in binary and ternary lithium silicate gels have been investigated for possible application as electrolytes in solid-state batteries and related electrochemical devices.[8-11] Ionic conductivities of $(LiCl)_2$–B_2O_3–SiO_2 xerogels have been reported previously by the authors.[10] In this study, the effect of a second glass former (B_2O_3) was studied. The ionic conductivity and structure of the corresponding $(LiCl)_2$–Al_2O_3–SiO_2 xerogels were investigated by ac impedance, powder X-ray diffraction, Fourier transform infrared (FTIR) spectroscopy, and ^7Li, ^{29}Si, and ^{27}Al solid-state NMR. While both Al_2O_3 and B_2O_3 introduce trivalent cations, the role of Al_2O_3 in a glass is considered to be an intermediate rather than a glass former (B_2O_3). The results of this study can be compared to the previous study to determine the role of the intermediate.

Experimental Section

The lithium aluminosilicate gels have been prepared by using experimental procedures similar to those used to prepare the lithium borosilicate gels.[10] The starting materials are tetraethylorthosilicate (TEOS, $Si(OCH_2CH_3)_4$) (Fisher, reagent), aluminum nitrate (Alfa, 99.999%), and lithium chloride (Alfa, 99.6%). After the gels were dried in a 65 °C oven for 2 weeks, they were heat treated at 525 °C for 10 h in an electric tube furnace under a flowing oxygen atmosphere.

Powder X-ray diffraction (PXRD) patterns were obtained with a SCINTAG PAD V diffractometer with monochromatized Cu Kα radiation. Elemental analysis for Li, Al, and Si were performed on a Beckman-Spectrametrics Spectraspan IIIB DCT Basic Multi dc-argon plasma emission spectrometer.

Fourier transform infrared (FTIR) spectra were recorded at room temperature on a Mattson Cygnus 100 FTIR spectrophotometer on xerogel powder dispersed in KBr pellets at room temperature in the range 520–4000 cm^{-1} with 2-cm^{-1} resolution.

^7Li, ^{29}Si, and ^{27}Al nuclear magnetic resonance (NMR) spectra were recorded on a Varian VXR-200 spectrometer equipped with a Doty magic angle spinning (MAS) probe. The resonance frequencies were 77.7 MHz for ^7Li, 39.8 MHz for ^{29}Si, and 52.1 MHz for ^{27}Al. The ^{27}Al and ^{29}Si MAS spectra were obtained using a simple one-pulse sequence with a 4.3-kHz spinning rate. The pulse flip angle used on the ^{27}Al spectra is 30°. The recycle time between pulses was 1 and 60 s, respectively, for ^{27}Al and ^{29}Si. Tetramethylsilane (TMS) and 0.1 M $AlCl_3$ aqueous solutions were used as NMR references for ^{29}Si and ^{27}Al. The static ^7Li spectra were

* Author to whom correspondence should be addressed.
† Also affiliated with the Department of Ceramics.

(1) Johnson, R. T., Jr.; Biefeld, R. M.; Knotek, M. L.; Morosin, B. *J. Electrochem. Soc.* **1976**, *123*, 680.
(2) Pechenik, A.; Susman, S.; Whitmore, D. H.; Ratner, M. A. *Solid State Ionics* **1986**, *18/19*, 403.
(3) Pechenik, A.; Whitmore, D. H.; Susman, S.; Ratner, M. A. *J. Non-Cryst. Solids* **1988**, *101*, 54.
(4) de Lambilly, H.; Klein, L. C. *J. Non-Cryst. Solids* **1989**, *109*, 69.
(5) de Lambilly, H.; Klein, L. C. *J. Non-Cryst. Solids* **1988**, *102*, 269.
(6) Anderson, P.; Klein, L. C. *J. Non-Cryst. Solids* **1987**, *93*, 415.
(7) Ho, S.; Klein, L.; Caracciolo, R. *J. Non-Cryst. Solids* **1990**, *120*, 267.
(8) Szu, S.; Greenblatt, M.; Klein, L. C. *Solid State Ionics* **1991**, *46*, 291.
(9) Tsai, M.; Szu, S.; Wang, B.; Greenblatt, M. *J. Non-Cryst. Solids*, in press.
(10) Wang, B.; Szu, S. P.; Tsai, M.; Greenblatt, M.; Klein, L. C. *Solid State Ionics* **1991**, *47*, 297.
(11) Klein, L. C.; Wakamatsu, H.; Szu, S.; Greenblatt, M. Submitted to Sixth International Workshops on Glasses and Ceramics from Gels, Seville, Spain, October 6–11, 1991.

0897-4756/92/2804-0191$03.00/0

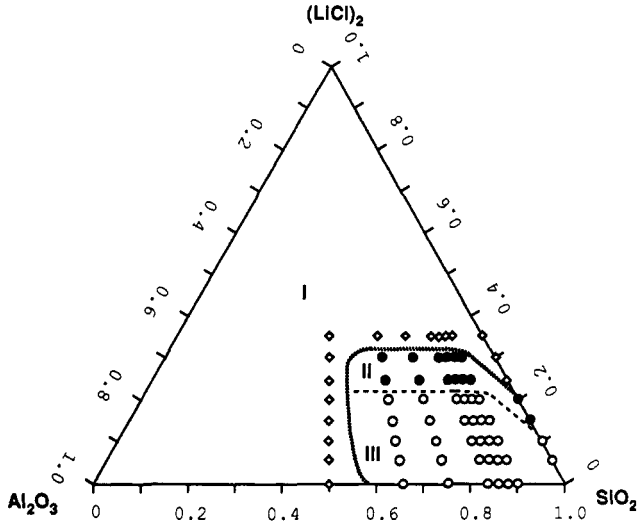

Figure 1. Gel-forming region in the $(LiCl)_2$–Al_2O_3–SiO_2 system: ◇, no monolithic gel formation or excess crystalline LiCl on the gel surface after drying for 2 weeks at 65 °C; ●, monolithic dried gels form after drying at 65 °C for 2 weeks, but gels partially crystallized after heat treatment at 525 °C for 10 h; ○, amorphous xerogels form after heat treatment at 525 °C for 10 h.

obtained with a solid-echo pulse sequence (90°-τ-90° data acquisition). The delay time (τ) between two 90° (10 μs) pulses was 20 μs and the recycle time was 60 s. The spin–lattice relaxation time (T_1) was measured using the inversion recovery method (180°-τ-90° data acquisition). All the heat-treated xerogels used for the NMR measurements were, unless stated otherwise, dried at 180 °C under vacuum (50 mTorr) for 12 h in a quartz tube. Samples were sealed in a quartz tube and then transferred to a drybox where they were packed in alumina (for ^{29}Si and ^{7}Li) or zirconia rotors (for ^{27}Al).

The ionic conductivities were measured by an ac complex impedance technique with a Solartron Model 1250 frequency analyzer and 1186 electrochemical interface that were programmed by a Hewlett-Packard 9816 desktop computer for data collection and analysis. The contact to the samples was made by coating the faces of sample plates with platinum paste. The frequency range 10 Hz to 65 kHz was employed at a heating rate 2 °C/min over the temperature range of 100–525 °C.

Results and Discussion

Figure 1 shows the gel-forming range in the $(LiCl)_2$–Al_2O_3–SiO_2 system. In region I, which corresponds to the samples containing more than 30 mol % $(LiCl)_2$ and/or the Al_2O_3/SiO_2 ratio higher than 1, either no monolithic gels formed or excess LiCl was found on the surface of the gels. In region II, with $(LiCl)_2$ content ranging from 25 to 30 mol % and the Al_2O_3/SiO_2 ratio less than 1, monolithic gels formed, but the gels partially crystallized after heat treatment at 525 °C for 10 h. In region III, with $(LiCl)_2$ less than about 25 mol % and Al_2O_3/SiO_2 ratio less than 1, amorphous xerogels were formed after heat treatment of the monolithic gels at 525 °C for 10 h. Eight heat-treated xerogels in region III were selected for ionic conductivities and structural studies. Five samples have the same lithium content (20 mol % $(LiCl)_2$) but different Al_2O_3/SiO_2 ratios (1/2 to 1/6), and the other three samples have a fixed Al_2O_3/SiO_2 ratio of 1/2 but different lithium content (5, 10, and 15 mol % $(LiCl)_2$) (Table I). These samples are labeled subsequently as $x(y)$, where x is the mole percent of $(LiCl)_2$ and y is the molar ratio of Al_2O_3/SiO_2. Elemental analyses of the xerogels for Li, Al, and Si show good agreement with their starting compositions (Table I).

Powder X-ray diffraction (PXRD) measurements for the selected gels show similar crystallization behavior. Figure 2 displays a typical PXRD of sample 20 (1/2) as a function of heat-treatment temperature. The 65 °C gel and 525 °C heat-treated xerogel were amorphous for X-rays. After heat treatment at 575 °C, the gel partially crystallized to $LiAlSi_3O_8$. The intensities of these diffraction peaks increased with the temperature of heat treatment.

Table I. Xerogel Starting Compositions (in Mole Percent)

sample	Al_2O_3/SiO_2	$(LiCl)_2$	Al_2O_3	SiO_2
5(1/2)	1/2	5	32	63
10(1/2)	1/2	10	30	60
15(1/2)	1/2	15	28	57
20(1/2)	1/2	20	27	53
20(1/3)	1/3	20	20	60
20(1/4)	1/4	20	16	64
20(1/5)	1/5	20	13	67
20(1/6)	1/6	20	11	69

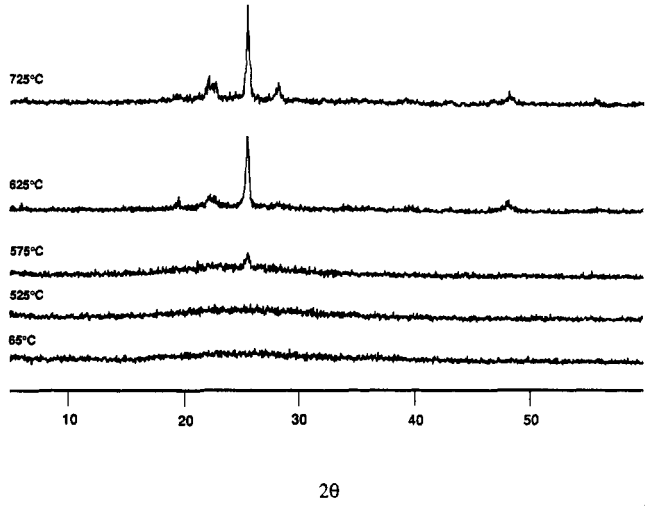

Figure 2. Powder X-ray diffraction patterns of sample 20(1/2) after heat treatment at various temperatures under flowing oxygen atmosphere. Diffraction peaks above 575 °C corresponds to $LiAlSi_3O_8$.

Figure 3 shows the FTIR spectra of xerogels with the same lithium content (20 mol % $(LiCl)_2$) but with different Al_2O_3/SiO_2 ratios (1/2 to 1/6). All the xerogels exhibit a strong peak at ≈1640 cm^{-1}, an absorption peak at ≈1070 cm^{-1}, a weak peak between 800 and 700 cm^{-1}, and another peak at ≈460 cm^{-1}. The assignments of FTIR absorption bands are based on those given in refs 12–15: H–O–H vibrations at ≈1640 cm^{-1}, asymmetric Si–O stretching at ≈1070 cm^{-1}, T–O vibrations of the TO_4 (T = Si, Al) tetrahedra around 700–800 cm^{-1}, Si–O–Si bending at ≈460 cm^{-1}.

The observed IR bands may be analyzed in terms of the composition. It is observed that as the Al_2O_3/SiO_2 ratio increases, the absorption peak at ≈1070 cm^{-1} gradually becomes broader due to the increasing aluminum perturbation of the Si–O stretching vibration.[12]

The band due to T–O vibrations of the TO_4 (T = Si, Al) tetrahedra shifts from 799 to 702 cm^{-1} and broadens considerably with increasing Al_2O_3/SiO_2 ratio. At low Al_2O_3 content the T–O bond vibration is more like the Si–O bond vibration in SiO_4. As the Al_2O_3/SiO_2 ratio increases, the T–O bond vibration becomes more like the Al–O vibration. Since the Al–O bond is longer than the Si–O bond and the force constant of the Al–O bond is smaller than that of the

(12) Roy, B. N. *J. Am. Ceram. Soc.* **1987**, *70*, 183.
(13) Brinker, C. J.; Scherer, G. W. *Sol-gel Science*; Academic Press: New York, 1990; pp 581.
(14) Murthy, M. K.; Kirby, E. M. *J. Am. Ceram. Soc.* **1962**, *45*, 324.
(15) Day, D. E.; Rindone, G. E. *J. Am. Ceram. Soc.* **1962**, *45*, 489.

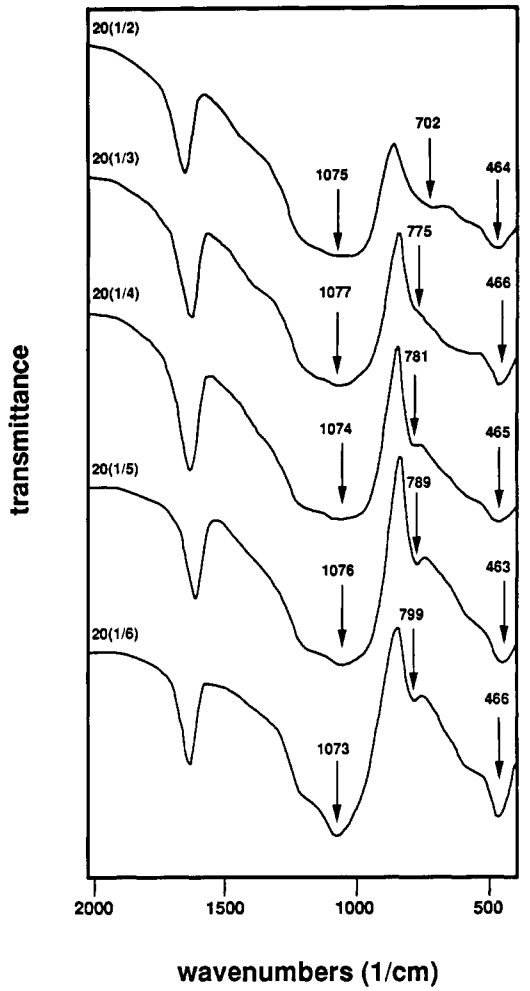

Figure 3. FTIR spectra of xerogels having 20 mol % $(LiCl)_2$ with different Al_2O_3/SiO_2 ratios.

Si–O bond, the T–O bond vibration shifts to lower frequency.[12] A similar trend is observed in the Li_2O–Al_2O_3–SiO_2 glass system.[12,13] This trend suggests that more and more Al isomorphously replaces Si in the tetrahedral position as the Al_2O_3/SiO_2 ratio increases. The shift of the Al–O vibration peak at $\approx$700 cm^{-1} and the broadening of the Si–O stretching peak at $\approx$1070 cm^{-1} are consistent with AlO_4 tetrahedra substitutionally replacing SiO_4 tetrahedra in the xerogel structure.

The 460-cm^{-1} band remained virtually insensitive to the compositional changes. This suggests that probably there is no significant change in the bending force constant of the Si–O–Si bond as the Al_2O_3/SiO_2 ratio changes.

Figure 4 displays the ^7Li NMR spectra of dried, heat-treated xerogels with a fixed lithium content (20 mol % $(LiCl)_2$) but with different Al_2O_3/SiO_2 ratios. All the spectra show an intense broad symmetric central peak with a narrower peak superimposed on top of the broader peak. In addition, under the central peak, there is another broad response. As the Al_2O_3/SiO_2 ratio decreases, the relative intensities of both the broad response and the superimposed narrow peak decrease.

Figure 5 shows the ^7Li NMR spectra of xerogels having different lithium contents with a fixed Al_2O_3/SiO_2 ratio of 1/2. The spectrum for sample 5(1/2) (bottom) displays a typical powder pattern of a first-order quadrupole interaction for a nucleus with spin $I = {}^3/_2$.[16] The broad

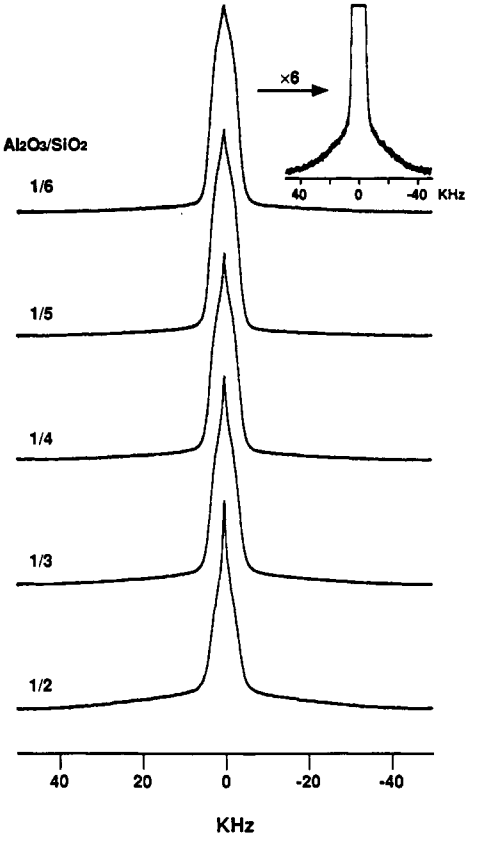

Figure 4. Static ^7Li NMR spectra for xerogels with the same lithium content (20 mol % $(LiCl)_2$) with different Al_2O_3/SiO_2 ratios (1/2 to 1/6). The inset shows the vertical expanded plot for sample with Al_2O_3/SiO_2 ratio of 1/6.

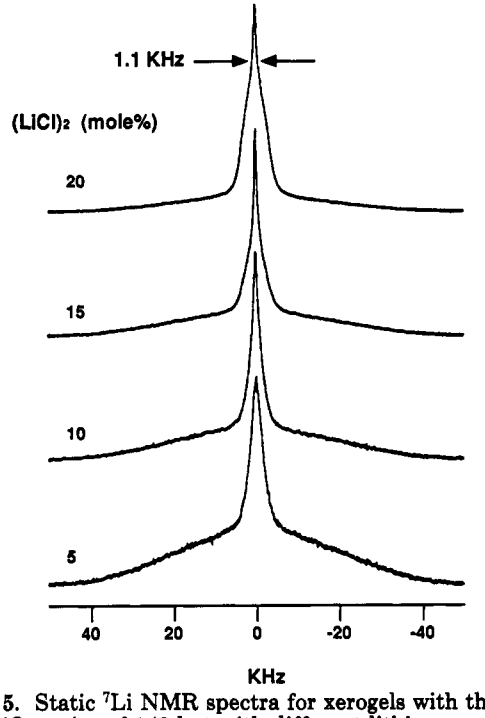

Figure 5. Static ^7Li NMR spectra for xerogels with the same Al_2O_3/SiO_2 ratios of 1/2 but with different lithium content.

response arises from the satellite transitions ($-{}^1/_2 \leftrightarrow -{}^3/_2$ and ${}^1/_2 \leftrightarrow {}^3/_2$) and the central peak arises from the central transition ($-{}^1/_2 \leftrightarrow {}^1/_2$). The shoulders and the divergences are smoothed out due to a distribution of the lithium environments. However, as the lithium content increases, the spectra become more similar to those shown in Figure 4, and the intensities of both the broad response (satellite

(16) Bray, P. J.; Gravina, S. J.; Hintenlang, D. H.; Mulkern, R. V. *Magn. Resn. Rev.* **1988**, *13*, 263.

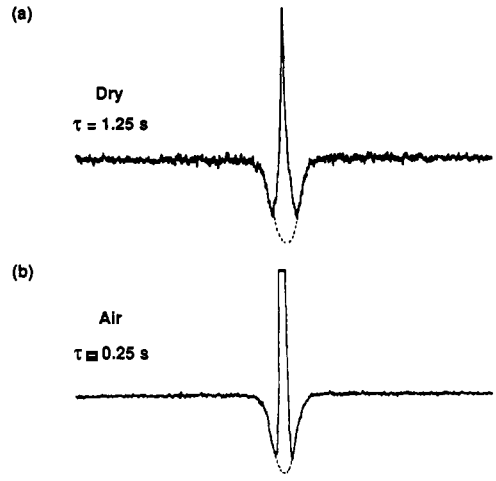

Figure 6. T_1 measurements for sample 20(1/2) (a) dried and (b) air exposed. τ is the delay time between the 180° and 90° pulses. The dashed curves are just for guiding the eyes.

transitions) and the top narrow peak (central transition) decrease. The ^{7}Li spectra shown in Figures 4 and 5 are attributed to the combined responses of two kinds of lithium ions.

The presence of two kinds of lithium species in the samples was confirmed by the T_1 measurements. The T_1 measurement for sample 20(1/2) clearly shows two relaxation processes. Figure 6a shows one of the spectra in the T_1 measurement for a delay time τ = 1.25 s. The up-pointed peak represents a faster relaxation process with T_1 estimated to be 0.8 s; the down-pointed peak corresponds to a slower relaxation process with T_1 estimated to be 3.6 s.

To further identify these two lithium species, both static ^{7}Li NMR and T_1 measurements were performed on an air-exposed sample 20(1/2). The static ^{7}Li spectrum for the air-exposed sample showed a dramatic decrease of the line width of the central peak (~250 Hz) compared to that of the sample under dry conditions (~7.7 kHz). However, the broad response was not affected by exposure to air. Similar results were found in the lithium borosilicate xerogels.[10] Analogous to the assignments made in the lithium borosilicate gels, one of the lithium species is assigned to lithium ions associated either with tetrahedral AlO_4 units or with nonbridging oxygens (NBO) in the silica network, where the lithium ions act as charge compensators (network-associated lithium). Similar to that observed in Li-containing glasses,[16] this kind of lithium ion gives the powder pattern of the first-order quadrupole interaction (i.e. the broad peak). The other kind of lithium species (i.e. the narrow peak) is assigned to polycrystalline LiCl since the line width of the narrow peak is comparable to that of the ^{7}Li spectrum of dried pure LiCl polycrystalline sample,[10] presumably dispersed in the pores of the gel. Because of its highly hygroscopic nature, the polycrystalline LiCl is hydrated once the sample is exposed to air and the hydrated $[Li(H_2O)_6]^+$ species are the source of the narrow NMR peak. The NMR line width of LiCl dissolved in water is identical to that of sample 20(1/2).

The T_1 measurement of the air-exposed sample supports these assignments for the lithium species. One of the spectra in the T_1 measurement for the air-exposed sample 20(1/2) is shown in Figure 6b. Again, two kinds of relaxation processes are evident. The narrow peak corresponds to hydrated lithium ions with a faster relaxation time (T_1 ~ 0.28 s) than the network-associated lithium species (T_1 ~ 0.58 s). The relaxation time, T_1, of the dried polycrystalline LiCl species is slower by about 1 order of

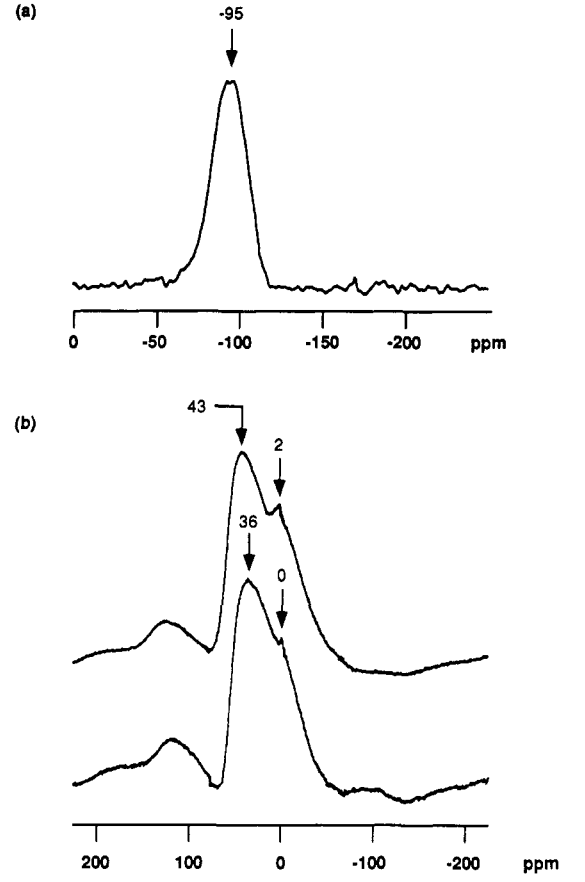

Figure 7. (a) ^{29}Si MAS NMR spectrum of dried xerogel 20(1/2). (b) ^{27}Al NMR spectrum of dried xerogels 20(1/2) and 20(1/6).

magnitude than that of the hydrated polycrystalline LiCl. This is due to the rapid rotation of water molecules around the lithium ions. In the xerogel, T_1 for the network-associated lithium ions decreases by about a factor of 2 when the sample is exposed to air. The change of the T_1 values between the dried and air-exposed samples is consistent with the above assignments for the two kinds of lithium species in the xerogel.

Although the ^{7}Li NMR indicates the presence of polycrystalline LiCl in the gels, X-ray diffraction failed to confirm the existence of LiCl. This is because X-ray diffraction experiments were carried out in the air, where water molecules can easily diffuse into the pores of the gel and associate with the highly hygroscopic polycrystalline LiCl grains to form hydrated LiCl.

On the basis of the assignment of the two lithium species, the change of the spectra in Figure 4 indicates that the number of lithium ions associated with silica (NBO) or alumina $[AlO_4]^-$ increases with an increasing Al_2O_3/SiO_2 ratio for samples with the same lithium content. The change in the spectra in Figure 5 indicates that the relative amounts of network-associated lithiums decrease with increasing lithium content for samples having a constant Al_2O_3/SiO_2 ratio.

The ^{29}Si NMR spectrum of sample 20(1/2) in Figure 7a shows an asymmetric peak around −95 ppm. The peak positions and the fwhh (full width at the half height intensity) of ^{29}Si NMR spectra for selected samples are listed in the Table II. As the lithium content or the Al_2O_3/SiO_2 ratio increases, the peak position shifts to less negative values (downfield) and the fwhh of ^{29}Si NMR spectra becomes wider (Table II). This is due to the increasing concentration of NBO on SiO_4^- with increasing lithium content. With increasing Al_2O_3/SiO_2 ratio, of course, more

Table II. Peak Positions and Fwhh of ^{29}Si Spectra

sample	peak position, ppm	fwhh, ppm
5(1/2)	−102 ± 1	22 ± 1
15(1/2)	−96 ± 1	25 ± 1
20(1/2)	−95 ± 1	25 ± 1
20(1/4)	−103 ± 1	23 ± 1
20(1/6)	−104 ± 1	20 ± 1

Table III. Conductivity Data of Xerogels

sample	$\sigma_{500°C}$, S/cm	E_a, eV
5(1/2)	2.9×10^{-5}	0.82 ± 0.05
10(1/2)	3.3×10^{-4}	0.68 ± 0.05
15(1/2)	3.4×10^{-3}	0.67 ± 0.05
20(1/2)	1.0×10^{-2}	0.67 ± 0.05
20(1/3)	7.5×10^{-3}	0.69 ± 0.05
20(1/4)	6.0×10^{-3}	0.81 ± 0.05
20(1/5)	5.4×10^{-3}	0.83 ± 0.05
20(1/6)	4.5×10^{-3}	0.86 ± 0.05

of the SiO_4 is replaced by AlO_4 tetrahedra. Both of these environmental changes around SiO_4 can move the chemical shift of ^{29}Si downfield.[17-19] At the same time, with increasing lithium and aluminum content, the distribution of the possible environments around a silicon tetrahedron is increased; hence, the fwhh of the ^{29}Si NMR peak increases with increasing lithium and aluminum content.[20] This is consistent with the result observed in FTIR where the peak around 1070 cm^{-1} broadens with increasing Al_2O_3/SiO_2 ratio due to the distribution of SiO_4 environment.

The ^{27}Al NMR spectra provide complementary information on the structure of lithium aluminosilicate xerogels. The ^{27}Al NMR spectra for samples 20(1/2) and 20(1/6) (Figure 7b) indicate two central peaks for both samples. The peaks at 2 and 0 ppm are assigned to octahedrally coordinated aluminum.[17,18] However, the environment of the peaks at 43 or 36 ppm is not certain. The position of the peaks is intermediate between four-coordinated aluminum where the shift is usually larger than 50 ppm[17,18] and five-coordinated aluminum where the shift is usually between 20 and 35 ppm.[21,22] The observed shift (δ_{exp}) is the combination of the real chemical shift (δ_{cs}) and the shift caused by the second-order quadrupole interaction (δ_Q) (i.e. $\delta_{cs} = \delta_{exp} + \delta_Q$);[23] the shift caused by the latter is proportional to the inverse square of the magnetic field. Hence, the correction of δ_Q should be considered when the ^{27}Al spectrum is measured at intermediate magnetic fields (4.7 T). The correction for δ_Q cannot be calculated in this study because the quadrupole coupling constant and the asymmetric parameter are not known. But, an approximation of this correction can be made, which gives a positive value of δ_Q so that the real chemical shift moves closer to the range expected for a four-coordinated aluminum. Previous reports of ^{27}Al NMR chemical shifts at 43 ppm assigned to tetrahedral AlO_4[24,25] support the assignment to AlO_4

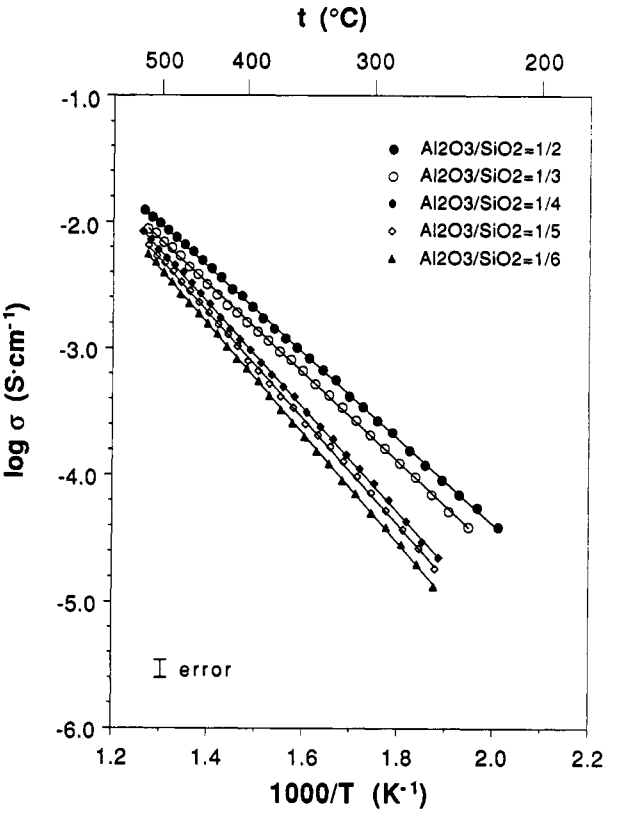

Figure 8. Arrhenius plots of the ionic conductivity for xerogels with the same lithium content (20 mol % $(LiCl)_2$) but with Al_2O_3/SiO_2 ratios varied from 1/2 to 1/6.

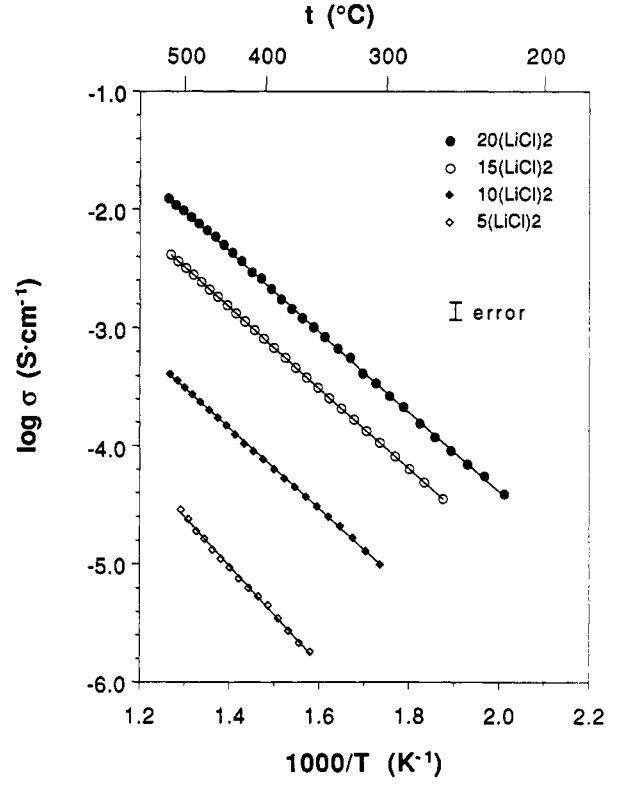

Figure 9. Arrhenius plots of the ionic conductivity for xerogels having different lithium content (5–20 mol % $(LiCl)_2$) at a fixed Al_2O_3/SiO_2 ratios of 1/2.

tetrahedra in our xerogels, as well. The FTIR spectra are consistent with the presence of four-coordinated aluminum. Since each AlO_4 requires one lithium ion for charge compensation, the assignment of peaks at 43 and 36 ppm

(17) Oestrike, S.; Yang, W. H.; Kirkpatrick, R. J.; Hervig, R.; Navrotsky, A.; Montez, B. *Geochim. Cosmochim. Acta* **1987**, *51*, 2199.
(18) Klinowski, *Prog. NMR Spectrosc.* **1984**, *16*, 237.
(19) Schramm, C. M.; de Jong, B. H. W. S.; Parziale, V. E. *J. Am. Chem. Soc.* **1984**, *106*, 4396.
(20) Prabakar, S.; Rao, K. J.; Rao, C. N. R. *J. Mater. Res.* **1991**, *6*, 592.
(21) Dupree, R.; Lewis, M. H.; Smith, M. E. *J. Appl. Crystallogr.* **1988**, *21*, 109.
(22) Risbud, S. H.; Kirkpatrick, R. J.; Taglialavore, A. P.; Montex, B. *J. Am. Ceram. Soc.* **1987**, *70*, c-10.
(23) Müller, D.; Jahn, E.; Ladwig, G.; Haubenreisser, U. *Chem. Phys. Lett.* **1984**, *109*, 332.
(24) Wu, Y.; Chmelka, B. F.; Pines, A.; Davis, M. E.; Grober, P. J.; Jacobs, P. A. *Nature*, **1990**, *346*, 550.
(25) Turner, G. L.; Kirkpatrick, R. J.; Risbud, R. H.; Oldfield, E. *Am. Ceram. Soc. Bull.* **1987**, *66*, 656.

to four-coordinated aluminum is consistent with the ^7Li NMR result which indicates the presence of network-associated lithium ions.

Ionic conductivity data for xerogels with the same lithium content but with different Al_2O_3/SiO_2 ratios (1/2 to 1/6) and samples having the same Al_2O_3/SiO_2 ratio of 1/2 but with different $(LiCl)_2$ content (5–20 mol %) are represented by Arrhenius plots in Figures 8 and 9, respectively. For all compositions, Arrhenius behavior is observed in the temperature range measured (200–525 °C). The activation energies and conductivities at 500 °C for these samples are collected in Table III.

Although the ^7Li NMR spectra indicate the presence of polycrystalline LiCl in these samples, the conducting mechanism appears to be different from that in pure polycrystalline LiCl.[10] Ionic compounds like LiCl contain a limited number of charge carriers, and their activation energy for conduction is the sum of both the energy for defect formation and the energy for defect migration. In contrast, most solid electrolytes have a large number of mobile ions with an activation energy, usually, representing only the energy needed for migration of defects.[26] The conducting behavior of lithium aluminosilicate xerogels is more similar to that seen in fast ionically conducting glasses.

For xerogels with increasing Al_2O_3/SiO_2 ratio and the same lithium content, the conductivity increases and the activation energy decreases, as shown in Figure 8 and Table III. As indicated by the ^7Li NMR spectra, for samples with high Al_2O_3/SiO_2 ratio, there are more lithium ions associated with NBO or the $[AlO_4]^-$ units. These lithium species are likely to be mobile and lead to high ionic conductivity and low activation energy. Similar results have also been observed in the lithium borosilicate xerogels.[10]

For xerogels with a fixed Al_2O_3/SiO_2 ratio of 1/2, the conductivity increases dramatically with increasing lithium content (Figure 9 and Table III). Parts a and c of Figure 10 show the conductivity and activation energy as a function of $(LiCl)_2$ content for xerogels at a fixed Al_2O_3/SiO_2 ratio of 1/2 at 500 °C. The conductivity is exponential in mole fraction of $(LiCl)_2$ as in most alkali oxide glasses.[27] The activation energy decreases rapidly when the $(LiCl)_2$ content increases from 5 to 10 mol %, then it remains nearly constant up to 20 mol % $(LiCl)_2$.

To understand this behavior, the variations of conductivity and activation energy with the lithium content were analyzed according to the Arrhenius equation

$$\sigma = \sigma_0 \exp\left(\frac{-E_a}{RT}\right) \tag{1}$$

where σ is conductivity, σ_0 is the preexponential term, and E_a is activation energy. The increasing conductivity from 5 to 10 mol % $(LiCl)_2$ is the combined effect of increasing preexponential factor and decreasing activation energy. While the increasing conductivity at high lithium content (10–20 mol % $(LiCl)_2$) is mainly due to the increasing preexponential factor (Figure 10b) since the activation energy is virtually constant.

According to the Anderson–Stuart model,[28] the activation energy for conduction E_a consists of two terms

$$E_a = \Delta E_B + E_S \tag{2}$$

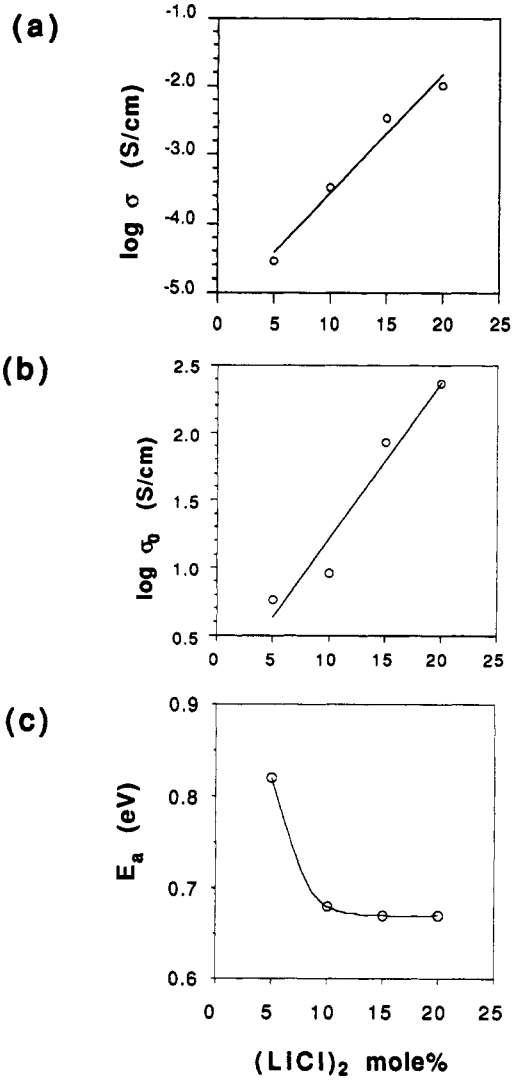

Figure 10. (a) Isotherms of conductivity as a function of mole fraction $(LiCl)_2$ for samples with a fixed Al_2O_3/SiO_2 ratio of 1/2. (b) log σ_0 as a function of mole fraction $(LiCl)_2$ for samples with a fixed Al_2O_3/SiO_2 ratio of 1/2. (c) Activation energy as a function of mole fraction $(LiCl)_2$ for samples with a fixed Al_2O_3/SiO_2 ratio of 1/2.

where ΔE_B represents the electrostatic interaction between the mobile ion and the host network and E_S is the elastic strain component. The electrostatic term ΔE_B has the form

$$\Delta E_B = \frac{zz_0e^2}{(r + r_0)} - \frac{zz_0e^2}{\lambda/2} \tag{3}$$

where ze and z_0e are the cation and oxygen charges; the radii of the mobile cations and oxygen are denoted by r and r_0, respectively; λ is the jump distance. The strain energy component is given explicitly by

$$E_S = 4\pi G r_D (r - r_D)^2 \tag{4}$$

where G is the modulus of the glass and r_D denotes the "doorway radius" (i.e. "bottle neck" or minimum window needed for motion of ion).

Since r_D does not change significantly with addition of modifier ions,[28,29] the change of E_S with increasing lithium content is negligible. Thus, the major contribution to the change of E_a is from ΔE_B. With increasing lithium content

(26) Collongues, R.; Kahn, A.; Michel, D. *Annu. Rev. Mater. Sci.* **1979**, *9*, 127.
(27) Tuller, H. L.; Button, D. P.; Uhlmann, D. R. *J. Non-Cryst. Solids* **1980**, *40*, 93.
(28) Anderson, O. L.; Stuart, D. A. *J. Am. Ceram. Soc.* **1954**, *37*, 573.
(29) Martin, S. W. *Solid State Ionics* **1986**, *18/19*, 472.

the fraction of lithium sites increases and the jump distance, λ, between lithium sites decreases. The decrease in jump distance, λ, decreases ΔE_B and E_a (eq 3). The decrease of activation energy with increasing lithium concentration from 5 to 10 mol % $(LiCl)_2$ is due to the decreasing jump distance with increasing lithium content.

At high lithium content (10–20 mol % $(LiCl)_2$), the term $zz_0e^2/(r + r_a)$ in ΔE_B, which describes the Coulombic interaction, increases with increasing lithium content and tends to increase E_a,[29] while the term $zz_0e^2/(\lambda/2)$ also increases with increasing lithium content (i.e. due to the decrease of λ) and tends to decrease E_a. The net result of this competition gives rise to the constant activation energy observed.

Conclusion

The gel-forming region of $(LiCl)_2$–Al_2O_3–SiO_2 xerogels is larger than the corresponding gel-forming region of $(LiCl)_2$–B_2O_3–SiO_2 xerogels. The ionic conductivity of lithium aluminosilicate xerogels is higher with an apparently different mechanism than the corresponding lithium borosilicate xerogels. For samples with constant lithium content (20 mol % $(LiCl)_2$) the ionic conductivity increases with increasing Al_2O_3/SiO_2 ratio due to increasing numbers of mobile lithium ions associated with AlO_4 units or nonbridging oxygens. In contrast, the conductivity in $(LiCl)_2$–B_2O_3–SiO_2 increases with decreasing B_2O_3/SiO_2 ratio due to increasing numbers of mobile lithium ions associated with BO_4 units or nonbridging oxygens.

For xerogels at a fixed Al_2O_3/SiO_2 ratio, the conductivity at 500 °C increases exponentially with the mole fraction of $(LiCl)_2$ and the activation energy decreases rapidly with the increasing $(LiCl)_2$ content from 5 to 10 mol % $(LiCl)_2$. However, E_a remains nearly constant as the $(LiCl)_2$ content increases from 10 to 20 mol %. This constant activation energy is analyzed in terms of the competition between the decreasing jump distance, which tends to decrease the activation energy, and the increasing Coulombic interaction, which tends to increase the activation energy.

Acknowledgment. This work was supported by the National Science Foundation—Materials Chemistry Program DMR 88-08234. We thank Dr. J. Elliot for the FTIR measurements.

Registry No. LiCl, 7447-41-8; Al_2O_3, 1344-28-1; SiO_2, 7631-86-9; ^7Li, 13982-05-3.

Role of Intermediate Phase Formation in the Preparation of $Ba_4Y_2O_7{\cdot}CO_2$†

D. A. Warner and R. E. Riman*

Department of Ceramics, Rutgers, The State University of New Jersey, Piscataway, New Jersey 08855-0909

Received May 24, 1991. Revised Manuscript Received September 3, 1991

The objective of this study was to determine the reaction conditions that facilitate optimal formation of $Ba_4Y_2O_7{\cdot}CO_2$, a compound useful for the preparation of the high-temperature superconductor $YBa_2Cu_3O_{7-x}$. $Ba_4Y_2O_7{\cdot}CO_2$ powders were prepared by conventional, colloid, and coprecipitation powder processing methods to assess the impact of the preparation technique and consequent particle mixing on the $Ba_4Y_2O_7{\cdot}CO_2$ formation mechanism and kinetics. The phase assemblage and phase purity were assessed as a function of solid-state reaction temperature (950–1150 °C) and soak time (2.5–20 h). Phase-pure $Ba_4Y_2O_7{\cdot}CO_2$ was prepared with a 20-h soak at 1050 °C. However, the powder synthesis method played no significant role in phase development. This surprising observation indicates that diffusion of the reactant species probably is not a factor in promoting formation of $Ba_4Y_2O_7{\cdot}CO_2$ as is observed in most solid-state reactions. Instead, $Ba_2Y_2O_5{\cdot}2CO_2$ intermediate phase formation segregates the system to the extent that the degree of homogeneity imparted by all three synthesis methods is equivalent. Formation of the $Ba_2Y_2O_5{\cdot}2CO_2$ intermediate may be related to nucleation and growth kinetics, which can be independent of the powder characteristics or mixedness of the system.

Introduction

Since the discovery of high-temperature superconductivity in the La–Ba–Cu–O system by Bednorz and Müller,[1] a number of oxide superconductors have been discovered.[2-6] The most widely studied oxide has been $YBa_2Cu_3O_{7-x}$, although it does not have the highest transition temperature.

While myriad chemical synthesis routes (e.g., sol–gel, coprecipitation, liquid mix) to prepare $YBa_2Cu_3O_{7-x}$ have been examined in the bulk state,[7-9] conventional powder processing appears able to prepare a material with similar superconducting properties. Thus, for economic reasons, conventional powder processing is the preferred route. However, conventional powder processing is not without drawbacks. A three-component mixture of powders (e.g., $BaCO_3$, CuO, and Y_2O_3) must be reacted at high temper-

† Presented at the 92nd Annual Meeting and Exposition of the American Ceramic Society, April 22–26, 1990, Indianapolis, IN.

(1) Bednorz, J. G.; Müller, K. A. *Z. Phys. B: Condensed Matter* **1986**, *64*, 189.
(2) Wu, M. K.; Ashburn, J. R.; Torng, C. J.; Hor, P. H.; Meng, R. L.; Gao, L.; Huang, Z. J.; Wang, Y. Q.; Chu, C. W. *Phys. Rev. Lett.* **1987**, *58*, 908.
(3) Hor, P. H.; Meng, R. L.; Wang, Y. Q.; Gao, L.; Huang, Z. J.; Bechtold, J.; Forster, K.; Chu, C. W. *Phys. Rev. Lett.* **1987**, *58*, 1891.
(4) Tarascon, J. M.; McKinnon, W. R.; Greene, L. H.; Hull, G. W.; Bagley, B. G.; Vogel, E. M.; Lepage, Y. *Adv. Ceram. Mater.* **1987**, *2* (3B), 498.
(5) Maeda, H.; Tanaka, Y.; Fukutomi, M.; Asano, T. *Jpn. J. Appl. Phys.* **1988**, *27*, L209.
(6) Sheng, Z. Z.; Kiehl, W.; Bennett, J.; El Ali, A.; Marsh, D.; Mooney, G. D.; Arammash, F.; Smith, J.; Viar, D.; Hermann, A. M. *Appl. Phys. Lett.* **1988**, *52*, 1738.
(7) Ritter, J. J. *Ceramic Transactions, Ceramic Powder Science II B*; *Vol. 1*, Messing, G. L., Fuller Jr., E. R., Hausner, H., Eds.; American Ceramic Society: Westerville, OH, 1988; pp 79–84.

0897-4756/92/2804-0197$03.00/0